



# Hollow nano-MgF<sub>2</sub> supported catalysts: Highly active and stable in gas-phase dehydrofluorination of 1,1,1,3,3-pentafluoropropane

Zhaohua Jia<sup>a,b</sup>, Wei Mao<sup>a,b,\*</sup>, Yanbo Bai<sup>a,b</sup>, Bo Wang<sup>a,b</sup>, Hui Ma<sup>a,b</sup>, Chen Li<sup>a,b</sup>, Jian Lu<sup>a,b,\*</sup>

<sup>a</sup> State Key Laboratory of Fluorine & Nitrogen Chemicals, Xi'an, Shaanxi 710065, China

<sup>b</sup> Xi'an Modern Chemistry Research Institute, Xi'an, Shaanxi 710065, China

## ARTICLE INFO

### Keywords:

Hollow nano-MgF<sub>2</sub>  
Lewis acidity  
Dehydrofluorination  
1,1,1,3,3-Pentafluoropropane  
1,3,3,3-Tetrafluoropropene

## ABSTRACT

In this work, different metal ions (Al<sup>3+</sup>, Cr<sup>3+</sup>, Fe<sup>3+</sup>, Co<sup>3+</sup>, Zn<sup>2+</sup>, Ni<sup>2+</sup>) were supported on a hollow nano-MgF<sub>2</sub> to catalyze gas-phase dehydrofluorination of 1,1,1,3,3-pentafluoropropane (HFC-245fa) to 1,3,3,3-tetrafluoropropene (HFO-1234ze). The support, hollow nano-MgF<sub>2</sub> prepared by a polyol mediated sol-gel method possesses large surface area (127 m<sup>2</sup> g<sup>-1</sup>) and mesoporous structure (12 nm) with weak Lewis acidity after calcination at 350 °C. The catalysts were characterized by TEM, XRD, BET, NH<sub>3</sub>-TPD, EDX, pyridine-IR and XPS. The physicochemical characterization showed via simple impregnation with different metal ions, the textural and surface acidic properties of hollow nano-MgF<sub>2</sub> were tuned, while the hollow nanosphere structure were maintained. The introduction of Al on hollow nano-MgF<sub>2</sub> has resulted in higher catalyst activity and selectivity to desired product, trans-1,3,3,3-tetrafluoropropene (HFO-1234ze(E)) than the other catalysts due to its largest surface area and numerous Lewis acid sites. The combination of the results of acidic properties and activity testing showed that the number of medium acid sites appeared to have a linear influence on the activity of hollow nano-MgF<sub>2</sub> supported catalysts. The highest activity with HFC-245fa conversion of 54% and 82% selectivity to HFO-1234ze(E) was obtained at 280 °C on hollow nano-MgF<sub>2</sub> supported 9 mol.% Al catalyst (9%Al/nano-MgF<sub>2</sub>), which also exhibited almost constant catalytic performances over 200 h. Surface Al species of Al/nano-MgF<sub>2</sub> catalysts were identified, including Al(OH)<sub>x</sub>F<sub>y</sub>/AlO<sub>x</sub>F<sub>y</sub>, β-AlF<sub>3</sub> and α-AlF<sub>3</sub>. The relative abundance of Al(OH)<sub>x</sub>F<sub>y</sub>/AlO<sub>x</sub>F<sub>y</sub> species was found to be highly correlated with the catalyst activity. The catalytic performances of 9%Al/nano-MgF<sub>2</sub> are significantly higher than those of traditional AlF<sub>3</sub> and fluorinated Cr<sub>2</sub>O<sub>3</sub> for gas-phase dehydrofluorination reactions.

## 1. Introduction

Fluorocarbons are indispensable functional chemicals in modern society as refrigerants, foam-forming agents, aerosol propellant, solvents, etc [1,2]. The evolution of fluorocarbons is motivated by environmental issues. Chlorofluorocarbons (CFCs), the first generation of fluorocarbons, have been banned to use by Montreal Protocol due to their destructive effects on the Earth's ozone layer. In response to climate change, hydrofluoroolefins (HFOs) are recently considered as the new alternatives to CFCs due to their low impacts to environment, such as low global warming potential (GWP) with zero ozone depletion potential [3,4]. In this regard, 1,3,3,3-tetrafluoropropene (HFO-1234ze), especially trans-1,3,3,3-tetrafluoropropene (HFO-1234ze(E)), has the potential to be used as one of the new environmentally-friendly fluorocarbons because of its special physical characteristics with much low GWP of 6 [5,6].

Recent years, it has been reported that HFO-1234ze can be conveniently prepared by gas-phase dehydrofluorination of 1,1,1,3,3-pentafluoropropane (HFC-245fa) over solid acid catalysts [7,8]. This reaction is typically carried out under high temperature and extreme corrosive conditions owing to thermodynamically endothermic characteristics and the formed HF [9]. As a consequence, the suitable catalytic materials are usually restricted to metal fluorides and fluorinated metal oxides, such as aluminum fluoride (AlF<sub>3</sub>) and fluorinated Cr<sub>2</sub>O<sub>3</sub> (F-Cr<sub>2</sub>O<sub>3</sub>). Although conventional AlF<sub>3</sub> and F-Cr<sub>2</sub>O<sub>3</sub> are active catalysts in the dehydrofluorination reactions, fast deactivation can be observed in these catalysts due to severe coke deposition on the strong acid sites. To improve the catalytic performance, Pd and Ni as the promoter are introduced into AlF<sub>3</sub> and F-Cr<sub>2</sub>O<sub>3</sub> catalysts, respectively [7,8]. However, satisfiable catalytic stability for industrial application still is not achieved. In view of intrinsically strong Lewis acidity, it is not a readily available process to tune finely the surface acidity of AlF<sub>3</sub> and F-Cr<sub>2</sub>O<sub>3</sub>.

\* Corresponding authors at: State Key Laboratory of Fluorine & Nitrogen Chemicals, Xi'an, Shaanxi 710065, China.

E-mail addresses: [hz\\_mw@163.com](mailto:hz_mw@163.com) (W. Mao), [lujian204@gmail.com](mailto:lujian204@gmail.com) (J. Lu).

<https://doi.org/10.1016/j.apcatb.2018.07.067>

Received 8 February 2018; Received in revised form 20 July 2018; Accepted 26 July 2018

Available online 26 July 2018

0926-3373/ © 2018 Elsevier B.V. All rights reserved.

catalysts. The air has to be added into the reaction system to prolong the catalytic stability. For instance, Ha et al. has reported that F-Cr<sub>2</sub>O<sub>3</sub> catalyst displays a relative steady activity over 50 h TOS at 1,1,1,2,3-pentafluoropropane/air = 10.0 (v/v) [10]. One US patent [11] also disclosed that a stable activity for F-Cr<sub>2</sub>O<sub>3</sub> catalyst was achieved over 360 h TOS when air (3% O<sub>2</sub> based on the HFC-245fa volume) was co-fed with HFC-245fa into the reactor. Nevertheless, the addition of air could lead to low selectivity, potential security problems and extra cost for separation. For these reasons, the design and fabrication of new catalyst materials is an urgent need for the preparation of HFOs by dehydrofluorination reactions in commercial processes.

Magnesium fluoride (MgF<sub>2</sub>), characteristic of high chemical inertness in harsh conditions and weak acid centers, make it an excellent catalytic support [12]. Over the years, MgF<sub>2</sub> as the support has been studied extensively in Cl/F exchange, hydrogenation, hydrodechlorination, hydrodesulfurization, photodegradation, ammoxidation, alkylation reactions, etc [12–20]. Regarding its weakly acidic surface [12], it is speculated that tuning finely the surface acidity by impregnation with different metal cations could be more feasible over the MgF<sub>2</sub> supported catalysts in comparison with the AlF<sub>3</sub> and F-Cr<sub>2</sub>O<sub>3</sub> catalysts. Unfortunately, to our knowledge, few academical articles have been reported on the gas-phase dehydrofluorination reactions over the MgF<sub>2</sub> supported catalysts. Very recently, Luo et al. has investigated the commercial MgF<sub>2</sub> supported catalysts in HFC-245fa dehydrofluorination, and found that pure commercial MgF<sub>2</sub> exhibited poor activity in this reaction and introducing V can improve the catalyst activity [21]. It is assumed that the poor textural stability at elevated temperature limits the application of MgF<sub>2</sub> supported catalysts in the high-temperature reactions. MgF<sub>2</sub> prepared by conventional liquid/gas-phase fluorination exhibits much low specific surface area (< 50 m<sup>2</sup> g<sup>-1</sup>) [22,23]. In general, it is an established fact that a support material provides a high surface area and a well-developed mesoporous structure which is essential for achieving a superior dispersion of active components and to favor the diffusion of reactants and products [24,25]. As a result, a number of new approaches have been developed to synthesize MgF<sub>2</sub> with high surface area (HS-MgF<sub>2</sub>, 70–300 m<sup>2</sup> g<sup>-1</sup>), including fluorolytic sol-gel, thermal decomposition of trifluoroacetate salts, SiO<sub>2</sub>-template fluorination, microemulsion method etc [23,26–29]. Although these HS-MgF<sub>2</sub> as supports or catalysts have shown excellent performance for synthesis of many fine chemicals [27,30], the microstructural stability of MgF<sub>2</sub> at elevated temperature (> 350 °C) is not substantially improved [22,31]. For example, the specific surface area of amorphous HS-MgF<sub>2</sub> decreases significantly from ~300 to ~40 m<sup>2</sup> g<sup>-1</sup> after calcination at 400 °C for several mins [22,23,28,31]. Therefore, for industrial applications in some high-temperature reactions, the development of novel HS-MgF<sub>2</sub> with excellent thermostability to fabricate appropriate catalysts is highly desirable but still remains a great challenge.

Recently, we have reported the preparation of crystalline *nano*-AlF<sub>3</sub> with high surface area by a polyol mediated sol-gel process [32], which exhibited excellent stability towards elevated temperature. In this process, the residual O derived from minor hydrolysis can resist the sintering of as-prepared metal fluorides under high-temperature treatment. Using the same methodology, crystalline *nano*-MgF<sub>2</sub> with hollow structure can be also prepared. The nanometer-sized hollow structure makes this material suitable for a wide range of applications, such as drug carriers, gas absorbents, catalytic materials, coating materials, and antireflective lenses [33,34]. More importantly, this hollow *nano*-MgF<sub>2</sub> is heat-tolerant to some extent, which displays a large specific surface area of 127 and 104 m<sup>2</sup> g<sup>-1</sup> even after calcination at 350 and 400 °C, respectively, for 5 h. In view of aforementioned advantages, the hollow *nano*-MgF<sub>2</sub> might be a good support for catalytic dehydrofluorination reactions.

In this work, we present a study on the catalytic behaviors of a series of hollow *nano*-MgF<sub>2</sub> supported catalysts (M/*nano*-MgF<sub>2</sub>, M = Al<sup>3+</sup>, Cr<sup>3+</sup>, Fe<sup>3+</sup>, Co<sup>3+</sup>, Zn<sup>2+</sup>, Ni<sup>2+</sup>) for gas-phase dehydrofluorination of

HFC-245fa. The present work aims to verify the feasibility of MgF<sub>2</sub> supported catalysts as an alternative to the current AlF<sub>3</sub> and F-Cr<sub>2</sub>O<sub>3</sub> catalysts in dehydrofluorination reactions. Especially, in view of increasingly strict environmental regulations, developing non-chromium catalysts based on the *nano*-MgF<sub>2</sub> is favorite in the F-industries nowadays. The hollow *nano*-MgF<sub>2</sub> supports were synthesized by a polyol mediated sol-gel method. It is expected that the impregnation with aforementioned metal ions could fabricate the hollow *nano*-MgF<sub>2</sub> supported catalysts with controlled surface acidity. And then the relationship of catalytic behavior and surface acidity was investigated in detail. Using FT-IR spectra of pyridine adsorption and NH<sub>3</sub>-TPD we have been able to measure the acidic properties of different hollow *nano*-MgF<sub>2</sub> supported catalysts. Furthermore, these catalysts were also characterized by XRD, EDX, TEM and BET method to address crystal, compositional, morphological, and textural changes, respectively.

## 2. Experimental

### 2.1. Preparation of hollow *nano*-MgF<sub>2</sub> supports and catalysts

The hollow *nano*-MgF<sub>2</sub> support was synthesized according to a polyol mediated sol-gel method [32]. Briefly, commercially available magnesium nitrate hexahydrate (Mg(NO<sub>3</sub>)<sub>2</sub>·6H<sub>2</sub>O, 99.9%) and polyethylene glycol (PEG2000) (Mw = 2000, 99.9%) were firstly dissolved in ethylene glycol (EG) (C<sub>2</sub>H<sub>6</sub>O<sub>2</sub>, 99.9%) under stirring at 60 °C; the concentration of [Mg<sup>2+</sup>] was 0.5 M and the mass ratio of PEG2000/EG was 1:10. Then, an aqueous solution of hydrogen fluoride (40 wt.%) was added stepwise into above solution under rigorous stirring for 6 h; hydrofluoric acid solution was used in the amounts enabling to result in 1:4 for Mg/F molar ratio. The as-prepared transparent and colourless sol was aged overnight at room temperature, and then transferred to an oven at 90 °C for 24 h to allow the formation of transparent wet gel. Finally, white gel powder of MgF<sub>2</sub> was obtained by drying the wet gel at 150 °C for 8 h.

The hollow *nano*-MgF<sub>2</sub> supported by different M (M = Al<sup>3+</sup>, Cr<sup>3+</sup>, Fe<sup>3+</sup>, Co<sup>3+</sup>, Zn<sup>2+</sup>, Ni<sup>2+</sup>) catalysts were prepared by the incipient wetness method. Firstly, the gel powder of MgF<sub>2</sub> (8.0–10.0 g) was impregnated by an ethanol solution of the corresponding metal nitrate hydrate (99.9%) with a desired amount. Unless otherwise stated, the content of the metal ions in the ethanol solution was adjusted to giving the final calculated metal loading 6 mol.% in the catalyst. Because of difference on solubility, the amount of ethanol solvent varied among 3.0–6.0 g so as to make different metal salts be dissolved. The prepared sample was aged overnight, then dried at 90 °C for 12 h, and finally calcined in air at 350 °C for 5 h with a heating rate of 1.5 °C min<sup>-1</sup>. For the sake of comparison, the unsupported MgF<sub>2</sub> catalysts were also prepared in the same way. All the raw materials were purchased from Sinopharm Chemical Reagent Co., Ltd. (China).

### 2.2. Catalytic reaction

The gas-phase dehydrofluorination of HFC-245fa (99%) provided by Xi'an Modern Chemistry Research Institute, was carried out at 280 °C under atmospheric pressure using a fixed-bed stainless steel reactor (1.0 cm inner diameter). Before reaction, 5 ml of prepared catalyst was loaded into the reactor and pretreated in N<sub>2</sub> at 280 °C for 0.5 h. Then the N<sub>2</sub> flow was stopped and HFC-245fa (0.05 mL/min) regulated by a high pressure constant flow pump (ELITE, P230II) was introduced into the reactor. The organic material was preheated in a vaporizer at 300 °C before being introduced into reactor. All pipes were heated by electricity and maintained at 45 °C to avoid the condensation of HFC-245fa. After the reaction the product gas was passed through a KOH solution to trap acid gases, then the gaseous products were analyzed by a gas chromatograph (SICT GC-2000III) equipped with a flame ionization detector (FID) and a GS-GASPRO capillary column (60 m × 0.32 mm).

The conversion of HFC-245fa and product selectivity was calculated

as defined:

$$\text{HFC-245fa conversion} = (\text{HFC-245fa}_{\text{in}} - \text{HFC-245fa}_{\text{out}}) / \text{HFC-245fa}_{\text{in}} \times 100\%$$

$$i_{\text{selectivity}} = i_{\text{out}} / (\text{HFC-245fa}_{\text{in}} - \text{HFC-245fa}_{\text{out}}) \times 100\%$$

Where *i* is HFO-1234ze(E) or HFO-1234ze(Z).

The activities of the catalysts were expressed as apparent rate ( $r_a$ ) or intrinsic rate ( $r_i$ ) calculated by the following equations:

$$r_a = F \times \text{HFC-245fa conversion} / m_{\text{cat}}$$

$$r_i = F \times \text{HFC-245fa conversion} / m_{\text{cat}} / S_{\text{cat}}$$

Where activity (reaction rate) is given in  $\text{mmol h}^{-1} \text{g}^{-1}$  or  $\text{mmol h}^{-1} \text{m}^{-2}$ , *F* is the molar flow rate of HFC-245fa ( $\text{mmol h}^{-1}$ ),  $m_{\text{cat}}$  is the amount of catalysts (g),  $S_{\text{cat}}$  is the surface area of catalysts ( $\text{m}^2 \text{g}^{-1}$ ).

### 2.3. Characterization

The specific surface area, total pore volume and the pore size distribution of the samples were measured by  $\text{N}_2$  physisorption at 77 K using Micromeritics ASAP 2020, determined by Brunauer-Emmett-Teller (BET) and Barret-Joyner-Halenda (BJH) desorption equation. Before the measurement, the samples were degassed at 250 °C for 10 h. X-ray diffraction (XRD) analyses were performed to detect the crystallized phases of the catalyst. The data were obtained using an Empyrean, PANalytical X-ray diffractometer equipped with Cu K $\alpha$  radiation ( $\lambda = 1.54056 \text{ \AA}$ ) at room temperature. The range of  $2\theta$  was 5°–90° with a step size of 0.02°. To determine the component in the catalyst along the surface cross-section, the signals of surface elements were detected by the energy-dispersive X-ray spectroscopy (EDX) (Oxford INCA Energy IE350) mapping method. The particle size and morphology of samples were observed using a transmission electron microscope (TEM, FEI Tecnai G2 F20, operated on 200 kv). The temperature-programmed desorption of ammonia ( $\text{NH}_3$ -TPD) measurement was carried on an AutoChem II 2920 instrument (Micromeritics, USA) for comparing the acidity of various samples. In a typical  $\text{NH}_3$ -TPD test, 0.1 g of sample was heated to 500 °C for 2 h in an Ar flow in a quartz reactor. After the temperature cooled to 110 °C in Ar, the sample was exposed to a  $\text{NH}_3$ -He (5%  $\text{NH}_3$ ) mixture for 60 min to allow the  $\text{NH}_3$  adsorption to complete. Then pure He was fed into the reactor for 2 h to purge physically adsorbed and free  $\text{NH}_3$ . After that, the sample was heated to 500 °C at a ramping rate of 10 °C  $\text{min}^{-1}$  under He flow. The desorbed  $\text{NH}_3$  was monitored by a mass spectra detector. The FTIR-photoacoustic spectroscopy of chemisorbed pyridine (Py-IR) was used to determine the nature of the acid sites (Lewis (L) and Brønsted (B) acid sites) by a PerkinElmer FT-IR Frontier spectrometer and a self-supported wafer of sample. The sample was pretreated at 350 °C for 1 h under vacuum prior to pyridine adsorption. Pyridine was adsorbed at room temperature from an argon flow for 0.5 h. Then, the samples were heated to 200 °C and evacuated to remove physisorbed and weakly chemisorbed pyridine. X-ray photoelectron spectroscopy (XPS) was used to analyze the change of the coordination state of surface element measured by Thermo Scientific K-Alpha equipment. The binding energy values were corrected for charging effect by referring to the adventitious C1s line at 284.8 eV.

## 3. Results and discussion

### 3.1. Characterization of hollow nano-MgF<sub>2</sub> supported catalysts

#### 3.1.1. Structural and textural properties of the catalysts

To determine the nano structures of as-prepared  $\text{MgF}_2$  particles including pure and supported by different metal after calcination at 350 °C, TEM analysis was conducted (Figs. 1,2). The images (Fig. 1a) show that the pure  $\text{MgF}_2$  particles are well-defined hollow nanospheres,

and the average diameter of nanospheres is 6.3 nm with the shell thickness of 1.7 nm. The high resolution TEM (HRTEM) results (Fig. 1b and c) for pure  $\text{MgF}_2$  particles exhibit that the identified lattice spaces of 0.227, 0.262 and 0.326 nm correspond to (111), (101) and (110) facets, respectively, of  $\text{MgF}_2$  [31,35], indicating the polycrystalline structure of prepared  $\text{MgF}_2$ . Fig. 2 shows the representative TEM images of different metal-supported  $\text{MgF}_2$  particles. As shown in Fig. 2a and b, the morphologies of Al/nano- $\text{MgF}_2$  and Cr/nano- $\text{MgF}_2$  are similar to that of pure hollow nano- $\text{MgF}_2$ . This means that the impregnation of hollow nano- $\text{MgF}_2$  with  $\text{Al}^{3+}$  and  $\text{Cr}^{3+}$  lead hardly to the significant change of hollow nano-structures. Furthermore, from the TEM images of Al/nano- $\text{MgF}_2$  and Cr/nano- $\text{MgF}_2$ , there is neither obvious interface between above active components and  $\text{MgF}_2$  particles nor obvious aggregation of active components occurring. However, the average diameter and the shell thickness of nanospheres increase slightly to 6.7 and 1.72 nm in above samples. These results indicate that above active components are highly dispersed on the hollow nano- $\text{MgF}_2$  even during the thermal treatment at elevated temperature. As revealed in Fig. 2c–f, the hollow nano-structures are also maintained in Zn/nano- $\text{MgF}_2$ , Fe/nano- $\text{MgF}_2$ , Ni/nano- $\text{MgF}_2$  and Co/nano- $\text{MgF}_2$ , and the nanoparticles with new morphologies are not observed. Although the average diameter of nanospheres varies slightly from 6.3 to 6.7 nm in Zn/nano- $\text{MgF}_2$ , Fe/nano- $\text{MgF}_2$  and Ni/nano- $\text{MgF}_2$ , the average diameter of Co/nano- $\text{MgF}_2$  increases remarkably to 8.7 nm. This means that the impregnation of hollow nano- $\text{MgF}_2$  with  $\text{Co}^{3+}$  results in the sintering of nanoparticles during the calcination process. In addition, the TEM-EDX mapping results (Supporting Information, Fig. S1) also clearly show that the elements Al, Cr, Zn, Fe and Ni, respectively, spread evenly in the whole nanoparticles, while partial aggregation can be observed for elemental Co in Co/nano- $\text{MgF}_2$ . This result reveals that the elemental Co can be not highly dispersed on hollow nano- $\text{MgF}_2$ .

The crystal structures of pure hollow nano- $\text{MgF}_2$  and various M/nano- $\text{MgF}_2$  were determined by XRD. It can be seen from Fig. 3 that all these samples show the diffraction peaks at 27.3°, 35.3°, 40.4°, 43.7°, 53.5°, 56.2°, 60.8° and 63.7°, corresponding to the characteristic diffraction peaks of  $\text{MgF}_2$  with rutile phase (JCPDS-41-1443) [36]. No diffraction peaks assigned to corresponding metal fluorides or oxides of supported metal are detected in all the samples. On basis of the TEM and TEM-EDX elemental mapping results, the elements Al, Cr, Zn, Fe and Ni, respectively, are highly dispersed on hollow nano- $\text{MgF}_2$ , which may account for no XRD diffraction peaks of these active components. Furthermore, Table 1 shows that the contents of supported metal detected by SEM-EDX (Fig S2) are much lower than the calculated loading, which can be attributed to active components loss during the preparation of catalyst. This is another possible reason for no diffraction peaks of these metal species. Especially, for Co/nano- $\text{MgF}_2$ , the content of Co detected by the SEM-EDX analysis is only 1.0 mol%. The low content is responsible to no diffraction peaks of Co species in Co/nano- $\text{MgF}_2$ , although partial aggregation can be observed for elemental Co from the TEM-EDX elemental mapping results.

To determine the textural properties of different M/nano- $\text{MgF}_2$  catalysts,  $\text{N}_2$  physisorption experiments were implemented. As shown in Fig. 4a, all the samples exhibit type IV isotherms with type H2 hysteric loops at high relative pressure according to the IUPAC classification, which is indicative of the presence of mesopores [26]. The H2 hysteresis loops at high relative pressure (0.8–1.0) are usually observed in the aggregate of particles with slit pores, which agree well with the TEM results. Moreover, the hysteresis loop of Al/nano- $\text{MgF}_2$  sample shifts to a lower relative pressure in contrast to other samples, implying a decline of the pore sizes. Based on the desorption branch of the isotherm, the pore size distribution was calculated by the BJH method. The results (Fig. 4b and c) display that all the samples contain narrow distribution of mesopores with a pore size of 7–12 nm. The mesoporous structure is vital to eliminate mass transfer resistance of reactants in and out of catalyst. Although no remarkable change occurs in the shape of isotherms after the introduction of different active

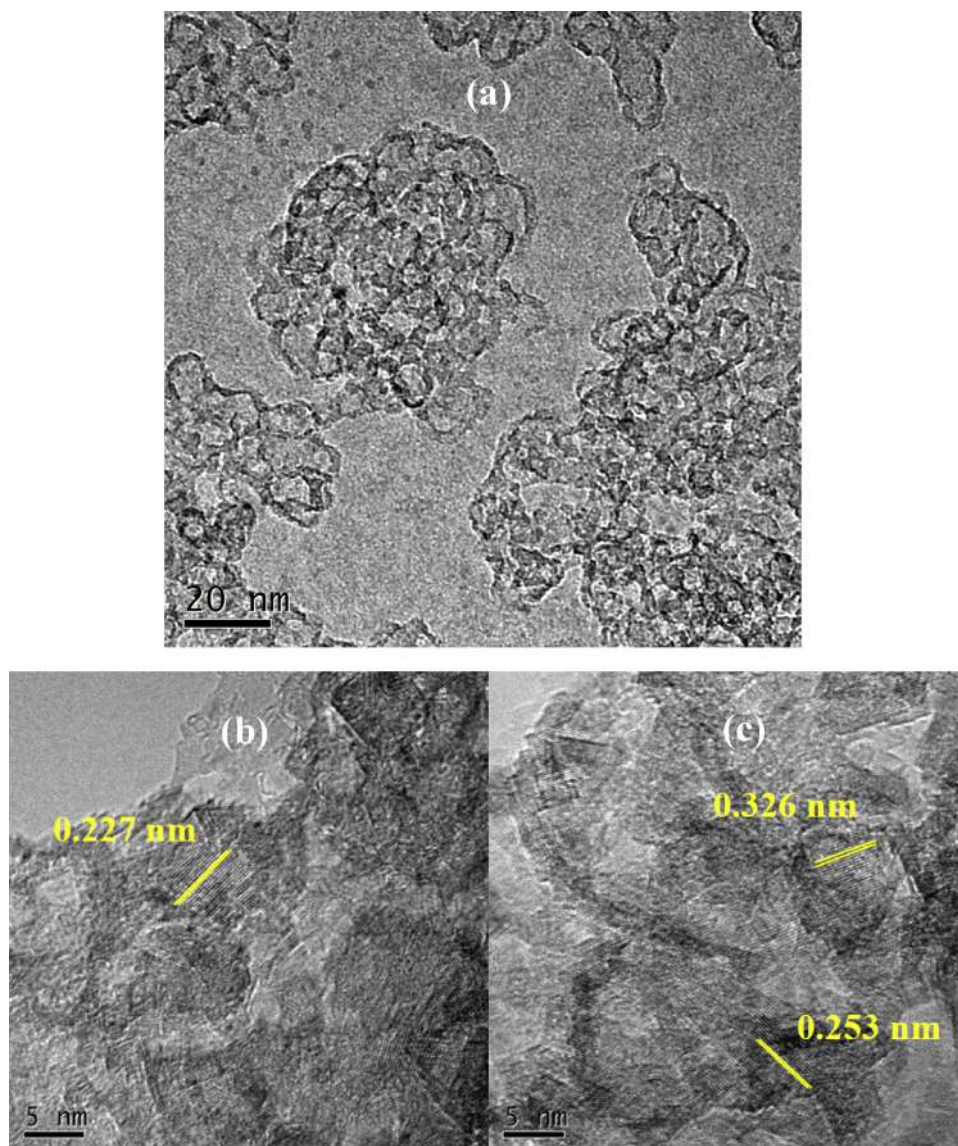


Fig. 1. Typical (a) TEM and (b, c) HRTEM images of pure  $\text{MgF}_2$  nanoparticles.

components on hollow *nano*- $\text{MgF}_2$ , the pore size decreases to some extent over various metal-supported hollow *nano*- $\text{MgF}_2$ . The textural properties were calculated and are summarized in Table 1. According to BET data given in Table 1, the BET surface area of hollow *nano*- $\text{MgF}_2$  is  $127 \text{ m}^2 \text{ g}^{-1}$  after calcination at  $350^\circ\text{C}$ , which is much higher than that of traditional  $\text{MgF}_2$  ( $< 50 \text{ m}^2 \text{ g}^{-1}$ ) [22,23]. The BET surface area is also larger than those of HS- $\text{MgF}_2$  prepared by  $\text{SiO}_2$ -template fluorination ( $92 \text{ m}^2 \text{ g}^{-1}$ ) [23] and thermal decomposition of trifluoroacetate salts ( $125 \text{ m}^2 \text{ g}^{-1}$ ) [28]. HS- $\text{MgF}_2$  prepared by fluorolytic sol-gel exhibits larger BET surface area than hollow *nano*- $\text{MgF}_2$ , but its BET surface area decreases to  $81 \text{ m}^2 \text{ g}^{-1}$  after treatment at  $300^\circ\text{C}$  [26]. On the other hand, the BET surface area can be remarkably increased to  $176 \text{ m}^2 \text{ g}^{-1}$  after the addition of  $\text{Al}^{3+}$  on hollow *nano*- $\text{MgF}_2$ . Fe/*nano*- $\text{MgF}_2$  sample also displays a slightly higher BET surface area than hollow *nano*- $\text{MgF}_2$ . With the impregnation of  $\text{Cr}^{3+}$ ,  $\text{Zn}^{2+}$  and  $\text{Ni}^{2+}$ , the BET surface area decreases a bit to  $100\text{--}120 \text{ m}^2 \text{ g}^{-1}$ . Notably, the BET surface area decreases significantly to  $51 \text{ m}^2 \text{ g}^{-1}$  after introducing  $\text{Co}^{3+}$  on hollow *nano*- $\text{MgF}_2$ . From the TEM analysis, high dispersion of Al species is achieved on hollow *nano*- $\text{MgF}_2$ , which is contributed to the large total surface area of Al/*nano*- $\text{MgF}_2$ . Except Co/*nano*- $\text{MgF}_2$ , the fluctuation of BET surface area on variant M/*nano*- $\text{MgF}_2$  can be probably attributed to the difference on the intrinsic BET surface area of different active

components, although they are highly dispersed on hollow *nano*- $\text{MgF}_2$ . In comparison with other M/*nano*- $\text{MgF}_2$ , partial aggregation of Co species and much larger particles are observed in Co/*nano*- $\text{MgF}_2$ , resulting in the lowest BET surface area among the prepared catalysts.

### 3.1.2. Acidic properties of the catalysts

Surface Lewis acid sites are believed as active sites for gas-phase dehydrofluorination reactions [37,38]. Thus, to clarify the nature of acid sites (Brønsted or Lewis) for M/*nano*- $\text{MgF}_2$  catalysts, IR absorption of adsorbed pyridine was performed. Pyridine adsorbed on Lewis acid sites (L-Py), yields two bands at  $\sim 1445$  and  $\sim 1610 \text{ cm}^{-1}$  whereas Brønsted acid sites (B-Py) are usually observed at  $\sim 1545$  and  $\sim 1640 \text{ cm}^{-1}$  [23]. As shown in Fig. 5, a weak absorption band at  $1446 \text{ cm}^{-1}$  is observed in hollow *nano*- $\text{MgF}_2$ , implying the number of Lewis acid sites is limited on this sample. Wojciechowska et al. have revealed that crystalline  $\text{MgF}_2$  hosts weak acid centers [12], which is supported by our results. By contrast, after introducing  $\text{Al}^{3+}$  and  $\text{Cr}^{3+}$  on hollow *nano*- $\text{MgF}_2$ , the intensity of absorption band at  $1446 \text{ cm}^{-1}$  is significantly enhanced. This indicates that a large amount of Lewis acid sites are present on Al/*nano*- $\text{MgF}_2$  and Cr/*nano*- $\text{MgF}_2$  samples. For Zn/*nano*- $\text{MgF}_2$ , Fe/*nano*- $\text{MgF}_2$  and Ni/*nano*- $\text{MgF}_2$ , the intensities of coordinated Py on Lewis acid sites at  $1610$  and  $1446 \text{ cm}^{-1}$  are also

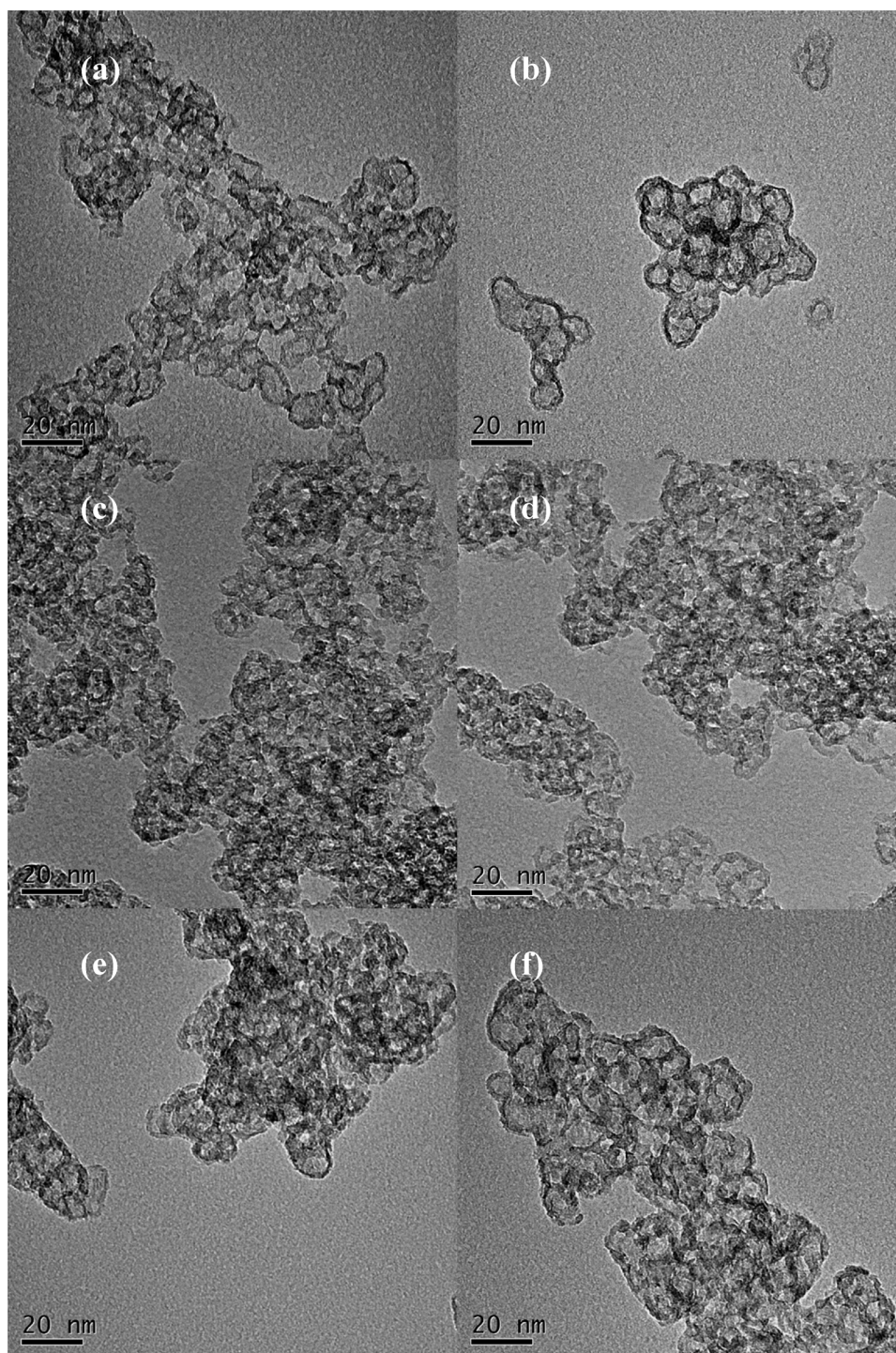


**Fig. 2.** TEM images of various M/nano-MgF<sub>2</sub> catalysts. (a) Al/nano-MgF<sub>2</sub>, (b) Cr/nano-MgF<sub>2</sub>, (c) Zn/nano-MgF<sub>2</sub>, (d) Fe/nano-MgF<sub>2</sub>, (e) Ni/nano-MgF<sub>2</sub> and (f) Co/nano-MgF<sub>2</sub>.

enhanced to some extent. Nevertheless, Co/nano-MgF<sub>2</sub> displays similar IR spectrum to hollow nano-MgF<sub>2</sub>, implying the number of Lewis acid sites is not improved after the addition of Co on hollow nano-MgF<sub>2</sub>. In addition, the absorption band at 1545 cm<sup>-1</sup> is not observed in each sample, which have shown that all the prepared catalysts possess no Brønsted acidity.

The total amount and the strength of acid sites for the hollow nano-MgF<sub>2</sub> supported catalysts were determined by NH<sub>3</sub>-TPD analysis. As seen in Fig. 6, a broad desorption peak of NH<sub>3</sub> appears in the temperature range from 130 to 350 °C on hollow nano-MgF<sub>2</sub>. The maximum

desorption peak centers around 190 °C, corresponding to weak acid sites, and a shoulder desorption peak corresponding to medium acid sites is also observed at 250 °C. The addition of Al<sup>3+</sup> into hollow nano-MgF<sub>2</sub> leads to a shift of the NH<sub>3</sub> desorption profile to a higher temperature (290 °C), indicating surface acidity is enhanced. However, the desorption profiles are similar for Cr/nano-MgF<sub>2</sub>, Zn/nano-MgF<sub>2</sub>, Fe/nano-MgF<sub>2</sub>, Ni/nano-MgF<sub>2</sub> and hollow nano-MgF<sub>2</sub> samples. This indicates that distribution of acid sites is not changed significantly after introducing Cr<sup>3+</sup>, Zn<sup>2+</sup>, Fe<sup>3+</sup> and Ni<sup>2+</sup> on hollow nano-MgF<sub>2</sub>. Notably, introducing Co<sup>3+</sup> on hollow nano-MgF<sub>2</sub> results in the reduction of the

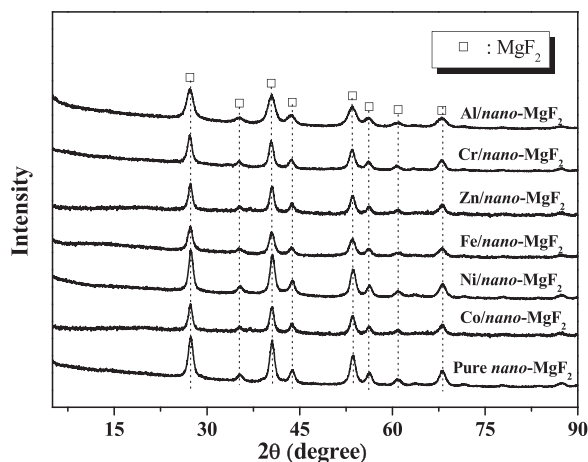


Fig. 3. XRD patterns of hollow *nano*-MgF<sub>2</sub> supported catalysts.

MS signals of NH<sub>3</sub> desorption peaks. As shown in Table 2, the total acid amount follows the decreasing order of Al/*nano*-MgF<sub>2</sub> > hollow *nano*-MgF<sub>2</sub> > Cr/*nano*-MgF<sub>2</sub> > Zn/*nano*-MgF<sub>2</sub> = Fe/*nano*-MgF<sub>2</sub> = Ni/*nano*-MgF<sub>2</sub> > Co/*nano*-MgF<sub>2</sub>. As expected, the addition of Al<sup>3+</sup> leads to the increase of the total amount and the strength of acid sites for hollow *nano*-MgF<sub>2</sub>, which can be ascribed to strong acidic properties of Al<sup>3+</sup> itself and improved surface area of catalyst. Interestingly, the total amount of acid sites for hollow *nano*-MgF<sub>2</sub> is not improved after the addition of Cr<sup>3+</sup>, which may be due to its relative lower surface area than pure hollow *nano*-MgF<sub>2</sub>. It is noteworthy that the number of Lewis acid sites is enhanced after the addition of Cr<sup>3+</sup> from the result of IR spectrum of pyridine chemisorption. Similar phenomena can be also observed in the Zn/*nano*-MgF<sub>2</sub>, Fe/*nano*-MgF<sub>2</sub> and Ni/*nano*-MgF<sub>2</sub>. To gain more insight, a semiquantitative comparison of the acidic distribution is performed by fitting the NH<sub>3</sub>-TPD curves using the Gaussian deconvolution method. Except Co/*nano*-MgF<sub>2</sub>, the number of medium acid sites is enhanced over the other M/*nano*-MgF<sub>2</sub> catalysts, which is coinciding with the increased number of Lewis acid sites. Indeed, pyridine is a strong base which is not adsorbed on acid site with weak strength. According to the TEM and BET results, the amount of acid sites for Co/*nano*-MgF<sub>2</sub> is much low owing to its large particle size, which results in few exposed surface acid sites.

### 3.2. Catalytic activity of hollow *nano*-MgF<sub>2</sub> supported catalysts

#### 3.2.1. Effect of supported metal

To investigate the effect of supported metal on the catalytic dehydrofluorination, HFC-245fa conversion, catalyst activity and HFO-1234ze selectivity over different catalysts are displayed in Table 3. Owing to limited Lewis acid sites, hollow *nano*-MgF<sub>2</sub> is not active in this reaction with a small conversion of HFC-245fa. Al/*nano*-MgF<sub>2</sub> exhibits the highest activity among the tested catalyst with regard to HFC-245fa

conversion and apparent reaction rate ( $r_a$ ), which is probably related to its numerous Lewis acidity. Concerning intrinsic reaction rate ( $r_i$ ), Cr/*nano*-MgF<sub>2</sub> is the most active catalyst, but in comparison with Al/*nano*-MgF<sub>2</sub>, the lower BET surface area and acidity amount restrict its apparent activity. Although the catalyst activity is also enhanced after introducing Zn<sup>2+</sup>, Fe<sup>3+</sup> and Ni<sup>2+</sup> on hollow *nano*-MgF<sub>2</sub>, their apparent activities are lower than those of Al/*nano*-MgF<sub>2</sub> and Cr/*nano*-MgF<sub>2</sub>. Co/*nano*-MgF<sub>2</sub> displays much poor catalytic activity, which is even lower than hollow *nano*-MgF<sub>2</sub>. This can be due to the lowest BET surface area and acidity amount of Co/*nano*-MgF<sub>2</sub> among the prepared catalysts. To gain a better understanding of how the Lewis acidity responds to catalyst activity, the apparent reaction rate is correlated with the number of medium acid sites for different M/*nano*-MgF<sub>2</sub> catalysts (Fig. 7). According to the results of acidic properties of catalysts, the increased Lewis acid sites over metal-supported hollow *nano*-MgF<sub>2</sub> mainly correspond to the number of medium acid sites determined by NH<sub>3</sub>-TPD. As shown in Fig. 7, an almost linear relationship is obtained between the amount of medium acid sites of M/*nano*-MgF<sub>2</sub> and apparent activity of catalyst. The largest amount of medium acid sites can be observed over the Al/*nano*-MgF<sub>2</sub> catalyst, corresponding to the optimal catalytic activity.

On the other hand, HFO-1234ze(E) and HFC-1234ze(Z) are the major products in the gas-phase dehydrofluorination of HFC-245fa, and the total selectivity to HFO-1234ze almost reaches to 99% over each catalyst except over Co/*nano*-MgF<sub>2</sub>. However, it must be emphasized that HFO-1234ze(E) is commercially more valuable than HFO-1234ze(Z) now. With regard to selectivity of HFO-1234ze(E), Al/*nano*-MgF<sub>2</sub> and Cr/*nano*-MgF<sub>2</sub> exhibit the highest catalytic performance among the tested catalysts. The variation of the distribution of cis, trans-isomers for HFO-1234ze is similar to the trend of catalyst's apparent activity. The best selectivity to HFO-1234ze(E) is also achieved over Al/*nano*-MgF<sub>2</sub>. Accordingly, it is reasonable to hypothesize that the medium acid sites of hollow *nano*-MgF<sub>2</sub> supported catalysts are responsible for the transformation of HFC-245fa to HFO-1234ze(E).

#### 3.2.2. Effect of Al loading and catalyst stability

Comprehensively, Al/*nano*-MgF<sub>2</sub> was selected as the optimized catalyst for our reaction system. To clear up the influence of Al<sup>3+</sup>, which exhibited the best activity for HFC-245fa dehydrofluorination over hollow *nano*-MgF<sub>2</sub> supported catalysts, the Al/*nano*-MgF<sub>2</sub> catalysts under different Al loading (calculated loading from 3 mol.% to 12 mol.%) were also prepared and tested in this reaction. As shown in Fig. 8, the HFC-245 conversion grows from 23% to 54% with the increase of Al content from 3 mol.% to 9 mol.%, then decreases slightly to 53% for 12%Al/*nano*-MgF<sub>2</sub>. Furthermore, as shown in Fig. S3, the  $r_a$  also increases from 2.53 to 4.97 mmol g<sup>-1</sup> h<sup>-1</sup> with the Al loading increasing from 3 mol.% to 9 mol.% and further addition of Al content leads to the  $r_a$  decreasing. A similar volcano plot between medium acidity amount of Al/*nano*-MgF<sub>2</sub> and Al loading is also observed with maximum centred at Al loading of 9 mol.%. This result suggests further that there is a close relationship between catalytic activity and medium acidity

Table 1

Chemical composition and textural properties of the M/*nano*-MgF<sub>2</sub> catalysts.

Catalyst	Supported metal loading (mol.%) <sup>a</sup>	Specific Surface area (m <sup>2</sup> g <sup>-1</sup> ) <sup>b</sup>	Total pore volume (cm <sup>3</sup> g <sup>-1</sup> ) <sup>c</sup>	Average pore size (nm)
hollow <i>nano</i> -MgF <sub>2</sub>	–	127	0.27	10.7
Al/ <i>nano</i> -MgF <sub>2</sub>	1.3	176	0.42	6.8
Fe/ <i>nano</i> -MgF <sub>2</sub>	2.2	131	0.39	8.4
Cr/ <i>nano</i> -MgF <sub>2</sub>	2.8	105	0.31	8.7
Zn/ <i>nano</i> -MgF <sub>2</sub>	1.0	117	0.36	9.0
Ni/ <i>nano</i> -MgF <sub>2</sub>	2.3	113	0.40	9.9
Co/ <i>nano</i> -MgF <sub>2</sub>	1.0	51	0.37	12.2

<sup>a</sup> Determined by the SEM-EDX analysis.

<sup>b</sup> BET method.

<sup>c</sup> Determined by N<sub>2</sub> volume adsorbed at p/p<sub>0</sub> = 0.99.

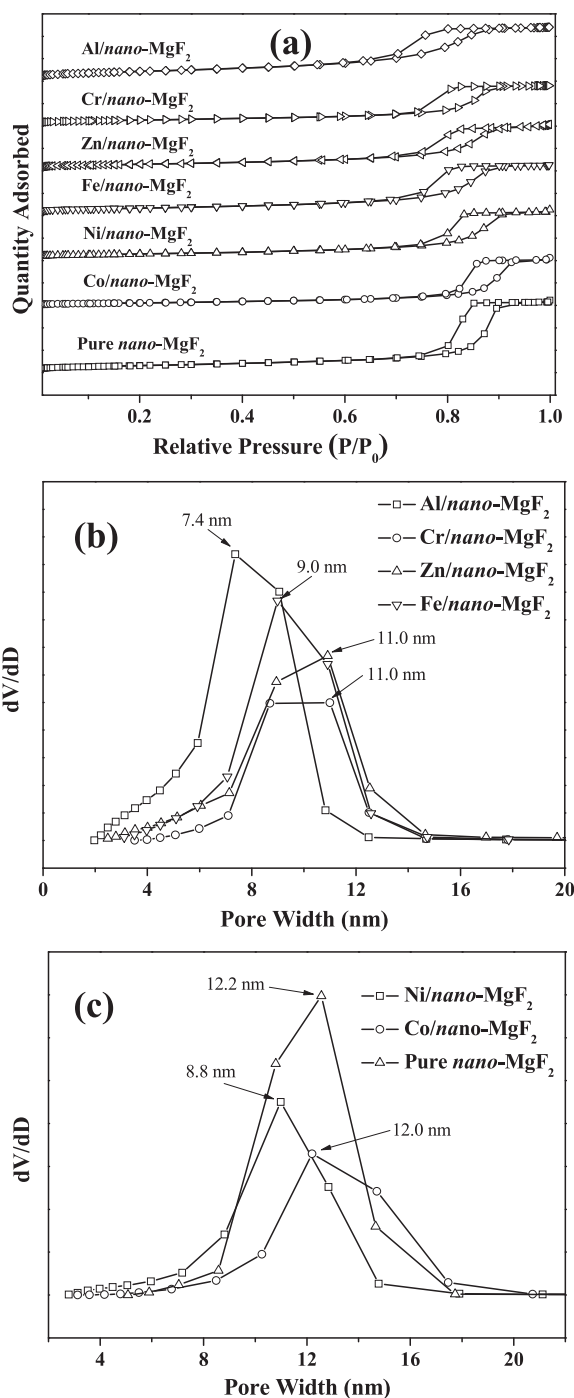


Fig. 4.  $N_2$  adsorption–desorption isotherms (a) and pore size distributions (b, c) for hollow  $nano-MgF_2$  supported catalysts.

amount of  $nano-MgF_2$  supported catalysts. However, the selectivity of HFO-1234ze(E) varies very small among 81%–82% over different Al/ $nano-MgF_2$  catalysts, independent of the Al loading. The observed catalytic performances indicate that the 9%Al/ $nano-MgF_2$  is the best active catalyst for gas-phase dehydrofluorination in our study. It is noteworthy that in the case of 9%Al/ $nano-MgF_2$ , the HFC-245fa conversion of 54% is much higher than those of traditional F-Cr<sub>2</sub>O<sub>3</sub> (conv. of 34.5%) and AlF<sub>3</sub> catalysts (conv. of 20%) at the same temperature reported by Luo et al. [7]; This conversion and the selectivity of HFO-1234ze(E) are also close to the values (conv. of 60.9% with selectivity of 83% to HFO-1234ze(E)) over their optimal Ni modified F-Cr<sub>2</sub>O<sub>3</sub> (15NiO/Cr<sub>2</sub>O<sub>3</sub>) catalysts. Consequently, our results confirm that the hollow  $nano-MgF_2$

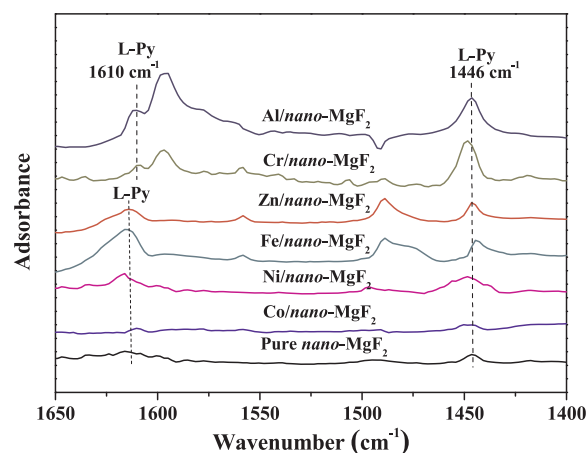


Fig. 5. IR spectra of pyridine adsorbed on hollow  $nano-MgF_2$  supported catalysts.

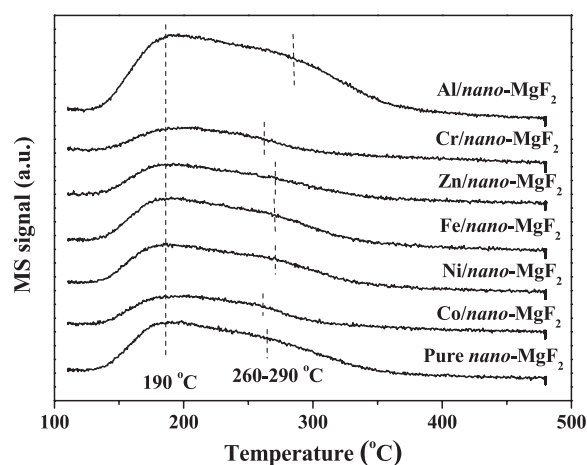


Fig. 6.  $NH_3$ -TPD profiles of hollow  $nano-MgF_2$  supported catalysts.

supported Al catalysts exhibit the great potential as an alternative to the traditional F-Cr<sub>2</sub>O<sub>3</sub> and AlF<sub>3</sub> catalysts in dehydrofluorination reactions.

The catalyst deactivation is the most troublesome problem in the gas-phase dehydrofluorination reactions at this moment. To examine the long-term behavior of catalyst under high HFC-245fa conversion, the activity of the 9%Al/ $nano-MgF_2$  catalysts for gas-phase dehydrofluorination was tested at 350 °C with the *LHSV* (HFC-245fa) of 0.6 h<sup>-1</sup> and the results are given in Fig. 9. High conversion is desirable in industry, which can reduce the circulation of material so as to save costs. Thus, the long-term behaviors of catalysts in the gas-phase dehydrofluorination reactions are usually performed at relative high temperature to obtain high conversion [7,8,10]. In the initial 48 h, the HFC-245fa conversion went down slightly with time from ~90% to ~88%, then the conversion slowed down and leveled off at 87%–88% over the rest of 200 h. The selectivity to HFO-1234ze(E) always maintained a high level at 82%–84%. Surprisingly, the 9%Al/ $nano-MgF_2$  catalysts presented good stability as reaction time went on among 200 h TOS, showing no deterioration in both conversion and selectivity. As described in Introduction, traditional AlF<sub>3</sub> and F-Cr<sub>2</sub>O<sub>3</sub> catalysts exhibit poor stability in this reaction, and the HFC-245fa conversion decreases remarkably within 24 h [7,8,10]; Even modified by Pd and Ni, traditional AlF<sub>3</sub> and F-Cr<sub>2</sub>O<sub>3</sub> based catalysts are still not stable over 100 h TOS. Although Luo et al. recently has reported that commercial  $MgF_2$  supported V catalyst exhibits good catalytic stability over 70 h TOS [21], they also point out that vanadyl fluorides are volatile and thus the catalyst stability during a long-term test could be a problem due to potential active component losing. Nevertheless, taking account the

**Table 2**  
Acidity amounts of hollow *nano*-MgF<sub>2</sub> supported catalysts.

Catalyst	Total acid sites <sup>a</sup> (mmol g <sup>-1</sup> )	Weak acid sites <sup>b</sup> (~190 °C) (mmol g <sup>-1</sup> )	Medium acid sites (mmol g <sup>-1</sup> )	
			(~250 °C)	(~310 °C)
Al/ <i>nano</i> -MgF <sub>2</sub>	0.25	0.115	0.087	0.048
Cr/ <i>nano</i> -MgF <sub>2</sub>	0.18	0.074	0.106	–
Zn/ <i>nano</i> -MgF <sub>2</sub>	0.16	0.074	0.086	–
Fe/ <i>nano</i> -MgF <sub>2</sub>	0.16	0.071	0.089	–
Ni/ <i>nano</i> -MgF <sub>2</sub>	0.16	0.079	0.081	–
Co/ <i>nano</i> -MgF <sub>2</sub>	0.12	0.072	0.048	–
Pure <i>nano</i> -MgF <sub>2</sub>	0.19	0.129	0.061	–

<sup>a</sup> Estimated from the integrated area under the MS signal curve of desorbed NH<sub>3</sub>.

<sup>b</sup> Calculated by the deconvoluted Gaussian lines from the normalized desorption peaks of NH<sub>3</sub>-TPD profiles.

**Table 3**  
Gas-phase dehydrofluorination of HFC-245fa over hollow *nano*-MgF<sub>2</sub> supported catalysts<sup>a</sup>.

Catalyst	Conv. of HFC-245fa (%)	Activity		Sel. (%)	
		r <sub>a</sub> (mmol h <sup>-1</sup> g <sup>-1</sup> )	r <sub>i</sub> (mmol h <sup>-1</sup> m <sup>-2</sup> )	HFO-1234ze(E)	HFO-1234ze(Z)
Al/ <i>nano</i> -MgF <sub>2</sub>	42.1	4.10	0.023	81.7	18.3
Cr/ <i>nano</i> -MgF <sub>2</sub>	36.0	3.53	0.034	81.5	18.5
Zn/ <i>nano</i> -MgF <sub>2</sub>	35.4	3.50	0.030	79.6	20.3
Fe/ <i>nano</i> -MgF <sub>2</sub>	27.2	2.00	0.015	79.9	20.0
Ni/ <i>nano</i> -MgF <sub>2</sub>	25.9	2.14	0.019	78.2	18.9
Co/ <i>nano</i> -MgF <sub>2</sub>	4.0	0.37	0.007	68.3	24.5
Pure <i>nano</i> -MgF <sub>2</sub>	7.9	0.66	0.005	74.2	25.8

<sup>a</sup> Reaction conditions: T = 280 °C, LHSV (HFC-245fa) = 0.6 h<sup>-1</sup>, atmospheric; data were collected after 200 reaction minutes.

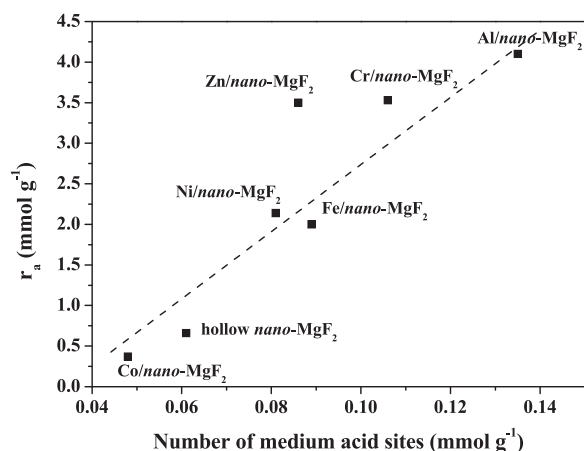


**Fig. 7.** The apparent reaction rates of M/*nano*-MgF<sub>2</sub> catalysts as a function of the number of medium acid sites.

potential difference of experimental setups between the different works in the literatures, the traditional AlF<sub>3</sub> and 9%Al/MgF<sub>2</sub> catalysts were also tested under the same reaction conditions as those for 9%Al/*nano*-

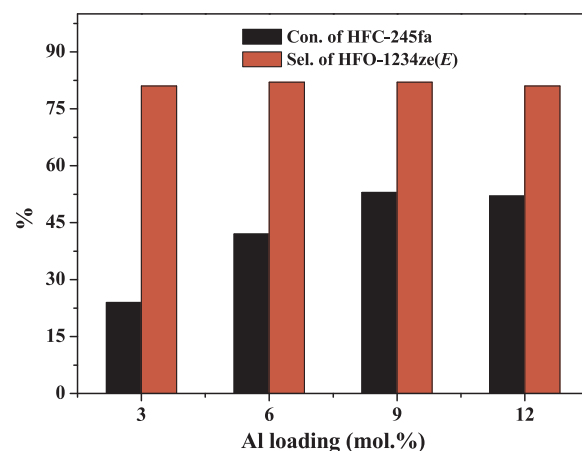


**Fig. 8.** Effect of Al loading on catalytic performance of Al/*nano*-MgF<sub>2</sub> (reaction conditions: T = 280 °C, LHSV (HFC-245fa) = 0.6 h<sup>-1</sup>, atmospheric).

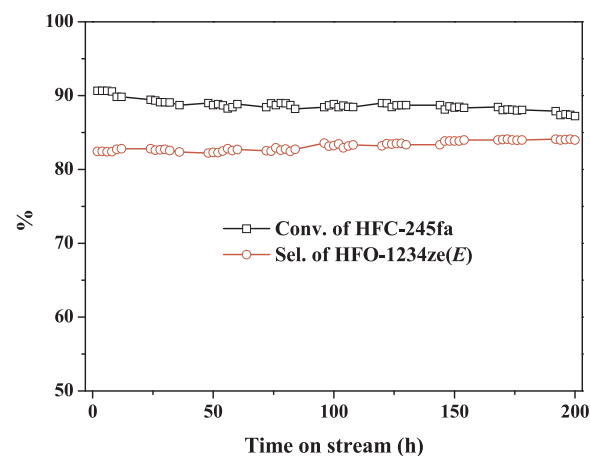


**Fig. 9.** Time on stream behavior of 9% Al/*nano*-MgF<sub>2</sub> catalysts in dehydrofluorination of HFC-245fa (reaction conditions: T = 350 °C, LHSV (HFC-245fa) = 0.6 h<sup>-1</sup>, atmospheric).

MgF<sub>2</sub>. Wherein, the traditional AlF<sub>3</sub> was prepared according to the method reported by Luo et al [8], and the traditional MgF<sub>2</sub> was prepared by reacting aqueous HF with MgO slurry in water and used as the support to prepare the 9%Al/MgF<sub>2</sub> catalysts. The long-term catalytic performances of these traditional catalysts are shown in Fig. S4. The TOS results display clearly that the catalytic lifetimes of traditional AlF<sub>3</sub> and 9%Al/MgF<sub>2</sub> are much shorter than that of 9%Al/*nano*-MgF<sub>2</sub>, although the initial HFC-245fa conversion are close on these catalysts. It should be noted that in terms of apparent reaction rate, the initial activity of 9%Al/*nano*-MgF<sub>2</sub> (8.5 mmol h<sup>-1</sup> g<sup>-1</sup>) is superior to those of the traditional AlF<sub>3</sub> (6.2 mmol h<sup>-1</sup> g<sup>-1</sup>) and 9%Al/MgF<sub>2</sub> (5.6 mmol h<sup>-1</sup> g<sup>-1</sup>). Furthermore, 9%Al/*nano*-MgF<sub>2</sub> also exhibits higher selectivity to HFO-1234ze(E), targeted product than the traditional catalysts regardless of reaction time. Concerning the catalytic behavior comprehensively, the 9%Al/*nano*-MgF<sub>2</sub> catalysts is much better than above traditional catalysts. Indeed, as revealed from the characterization results, the large surface area, mesoporous structure and medium acidity might exert a significant effect both on the catalytic activity and stability of Al/*nano*-MgF<sub>2</sub> catalysts. Combined with the results of catalyst activity, we could conclude that the hollow *nano*-MgF<sub>2</sub> supported Al catalyst is a very good sign of its applications in the F-industry, especially for the gas-phase dehydrofluorination reactions.

**Table 4**  
Peak deconvolution results of Al 2p XPS spectrum for different Al/nano-MgF<sub>2</sub> catalysts.

Sample	B. E. for Al 2p (eV)		
	Al(OH) <sub>x</sub> F <sub>y</sub> /AlO <sub>x</sub> F <sub>y</sub>	β-AlF <sub>3</sub>	α-AlF <sub>3</sub>
3%Al/nano-MgF <sub>2</sub>	74.2 (16.9%) <sup>a</sup>	75.4 (48.5%)	76.9 (34.6%)
6%Al/nano-MgF <sub>2</sub>	74.3 (27.1%)	75.5 (44.0%)	76.4 (28.9%)
9%Al/nano-MgF <sub>2</sub>	74.7 (34.4%)	75.7 (31.8%)	76.6 (33.8%)
9%Al/nano-MgF <sub>2</sub> (used)	75.0 (36.3%)	76.0 (37.1%)	76.7 (26.6%)
12%Al/nano-MgF <sub>2</sub>	75.0 (41.3%)	76.0 (42.7%)	76.9 (16.0%)

<sup>a</sup> Content of Al species in brackets.

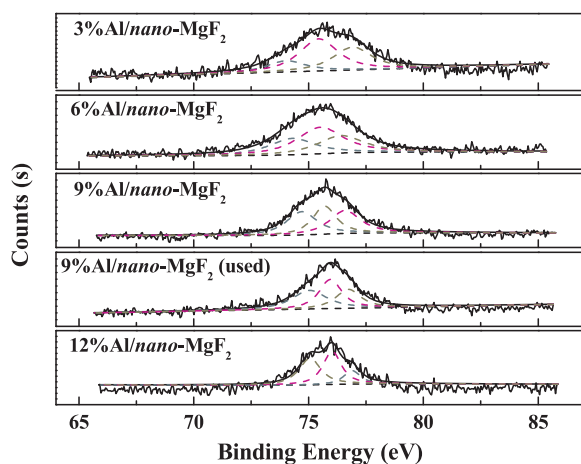


**Fig. 10.** XPS spectra of the Al 2p core-level for Al/nano-MgF<sub>2</sub> catalysts with different Al loading and used 9%Al/nano-MgF<sub>2</sub>.

### 3.3. Possible active species of Al/nano-MgF<sub>2</sub> catalysts

Based on above results, it is well recognized that Al/nano-MgF<sub>2</sub> is an active and stable catalyst for dehydrofluorination reactions, and its catalytic performance depends on the loading of Al. However, from TEM (Fig. S5) and XRD (Fig. S6) analyses, no remarkable change in the morphology and bulk structure is observed for variant Al/nano-MgF<sub>2</sub> catalysts with the Al loading from 3%–12%. The hollow nanosphere structure and the diffraction peaks of MgF<sub>2</sub> display in each sample. The TEM-EDX mapping results (Fig. S7) also reveal that the element Al is highly dispersed on nano-MgF<sub>2</sub> even at high Al loading. Based on above results, it can be concluded that the hollow nano-MgF<sub>2</sub> promote the dispersion of Al species under a broad range of Al loading. As shown in Table S1, increasing the Al loading, the BET surface area varies very small for different Al/nano-MgF<sub>2</sub> catalysts except 3%Al/nano-MgF<sub>2</sub>, and the particle size also varies slightly among 6.7–7.9 nm for these samples. Nevertheless, it should be noted that the acidity amount changes obviously with the increase of Al loading, which affects strongly its catalytic properties as revealed in abovementioned description. What is not known, however, is the Al species at the surface of the hollow nano-MgF<sub>2</sub>. To determine the nature of Al species active in dehydrofluorination reactions, XPS spectra were used to identify the surface Al species of different catalysts. As shown in Fig. 9, the Al 2p XPS spectra are similar in variant Al/nano-MgF<sub>2</sub> catalysts with the Al loading from 3%–12%, indicating surface species are similar over these samples. Considering the high corrosion of HF formed in the reaction, the Al 2p XPS spectrum of 9%Al/nano-MgF<sub>2</sub> reacted after 8 h was also detected. By comparison, there is no significantly change for Al 2p XPS spectrum between the fresh and used 9%Al/nano-MgF<sub>2</sub> catalysts. This can be ascribed to the formation of relative stable Al species at harsh conditions in the fresh catalyst. Each XPS spectrum of Al 2p on the Al/nano-MgF<sub>2</sub> catalysts can be deconvoluted into three peaks at about

74.2–75.0, 75.4–76.0 and 76.4–76.9 eV, which can be assigned to Al(OH)<sub>x</sub>F<sub>y</sub>/AlO<sub>x</sub>F<sub>y</sub>, β-AlF<sub>3</sub> and α-AlF<sub>3</sub>, respectively [39–41]. The XPS data obtained by applying a peak-fitting program are listed in Table 4. Interestingly, the content of Al(OH)<sub>x</sub>F<sub>y</sub>/AlO<sub>x</sub>F<sub>y</sub> increases with the enhancement of Al loading, the trend of which broadly coincides with the trend of catalytic activity except for 12%Al/nano-MgF<sub>2</sub>. Hence, surface Al(OH)<sub>x</sub>F<sub>y</sub>/AlO<sub>x</sub>F<sub>y</sub> can be considered as the main active species in Al/nano-MgF<sub>2</sub> catalysts for dehydrofluorination reactions. Considering the difference on catalytic activity and content of Al species, the structure of Al(OH)<sub>x</sub>F<sub>y</sub>/AlO<sub>x</sub>F<sub>y</sub> species formed on catalyst could be different between 12%Al/nano-MgF<sub>2</sub> and other Al/nano-MgF<sub>2</sub> catalysts. However, the exact nature of Al species active in this reaction needs further studying by in-situ characterization and theoretical chemistry (Fig. 10).

## 4. Conclusions

Overall, a series of hollow nano-MgF<sub>2</sub> supported catalysts (active component: Al<sup>3+</sup>, Cr<sup>3+</sup>, Fe<sup>3+</sup>, Co<sup>3+</sup>, Zn<sup>2+</sup>, Ni<sup>2+</sup>) were prepared and used for gas-phase dehydrofluorination of HFC-245fa. The support, hollow nano-MgF<sub>2</sub> was prepared by a novel polyol mediated sol-gel method, which displayed a large specific surface area of 127 m<sup>2</sup> g<sup>-1</sup> even after the high-temperature treatment of 350 °C, making it as a suitable catalytic support for gas-phase dehydrofluorination. The introduction of different metal on hollow nano-MgF<sub>2</sub> leads to the variation of the textural and surface acidic properties of catalysts, although each metal is highly dispersed on this material. The activity and selectivity of hollow nano-MgF<sub>2</sub> supported catalysts have been shown to be influenced by the number of the Lewis acid sites and the surface area of catalysts. Our results indicate that the presence of Al on the hollow nano-MgF<sub>2</sub> is best for catalytic transformation of HFC-245fa to HFO-1234ze(E), which can be due to its largest surface area and Lewis acidity amount among the prepared catalysts. The optimized Al/nano-MgF<sub>2</sub> catalysts with an Al loading of 9 mol.% achieve the best catalytic performances in a HFC-245fa conversion of 54% with a selectivity of 82% to HFO-1234ze(E) at 280 °C, the results of which are similar to the traditional F-Cr<sub>2</sub>O<sub>3</sub> based catalysts. More importantly, over 200 h tested, the 9%Al/nano-MgF<sub>2</sub> shows almost constant catalyst activity and selectivity to HFO-1234ze(E), which seems to meet the industrial applications in the gas-phase dehydrofluorination reactions for production of HFOs.

## Acknowledgments

This work was financially supported by Natural Science Basic Research Planning Shaanxi Province of China (No. 2017ZDJC-29), Shaanxi Province Science and Technology Innovation Project (No. 2016KTCL-15), Key Research and Development Project of Shaanxi Province (No. 2018ZDXM-GY-173).

## Appendix A. Supplementary data

Supplementary material related to this article can be found, in the online version, at doi:<https://doi.org/10.1016/j.apcatb.2018.07.067>.

## References

- [1] L.E. Manzer, *Science* 249 (1990) 31–35.
- [2] S.K. Ritter, *Chem. Eng. News* 91 (2013) 27–28.
- [3] G.J. Velders, A.R. Ravishankara, M.K. Miller, M.J. Molina, J. Alcamo, J.S. Daniel, D.W. Fahey, S.A. Montzka, S. Reimann, *Science* 335 (2012) 922–923.
- [4] M.K. Vollmer, S. Reimann, M. Hill, D. Brunner, *Environ. Sci. Technol.* 49 (2015) 2703–2708.
- [5] A. Mota-Babiloni, J. Navarro-Esbrí, F. Molés, Á.B. Cervera, B. Peris, G. Verdú, *Appl. Therm. Eng.* 95 (2016) 211–222.
- [6] Z. Yang, X. Wu, T. Tian, *Energy* 91 (2015) 386–392.
- [7] J.W. Luo, J.D. Song, W.Z. Jia, Z.Y. Pu, J.Q. Lu, M.F. Luo, *Appl. Surf. Sci.* 433 (2018) 904–913.
- [8] F. Wang, W.X. Zhang, Y. Liang, Y.J. Wang, J.Q. Lu, M.F. Luo, *Chem. Res. Chin.*

- Univ. 31 (6) (2015) 1003–1006.
- [9] J.W. Luo, Y. Liang, W.X. Zhang, B.T. Teng, Y.J. Wang, M.F. Luo, *Org. Fluor. Ind.* 2 (2015) 1–6.
- [10] S. Lim, M.S. Kim, J.W. Choi, H. Kim, B.S. Ahn, S.D. Lee, H. Lee, C.S. Kim, D.J. Suh, J.M. Ha, K.H. Song, *Catal. Today* 293–294 (2017) 42–48.
- [11] M. Y. Elsheikh, P. D. Fellenger, **US patent 6124510, 2000.**
- [12] M. Wojciechowska, M. Zieliński, M. Pietrowski, *J. Fluorine Chem.* 120 (2003) 1–11.
- [13] M. Zieliński, M. Pietrowski, A. Kiderys, M. Kot, E. Alwin, *J. Fluorine Chem.* 195 (2017) 18–25.
- [14] M. Pietrowski, M. Zieliński, M. Wojciechowska, *ChemCatChem* 3 (2011) 835–838.
- [15] A. Negoii, S. Wuttke, E. Kemnitz, D. Macovei, V.I. Parvulescu, C.M. Teodorescu, S.M. Coman, *Angew. Chem. Int. Ed.* 49 (2010) 8134–8138.
- [16] A. Malinowski, W. Juszczak, J. Pielaszek, M. Bonarowska, M. Wojciechowska, Z. Karpiński, *Chem. Commun.* (1999) 685–686.
- [17] A. Wajnert, M. Wojciechowska, M. Pietrowski, W. Przystajko, *Catal. Commun.* 9 (2008) 1493–1496.
- [18] F. Chen, H. Huang, X.P. Zhou, *J. Phys. Chem. C* 113 (2009) 21106–21113.
- [19] V.N. Kalevaru, B.D. Raju, V.V. Rao, A. Martin, *Appl. Catal. A Gen.* 352 (2009) 223–233.
- [20] F. Richard, S. Célérier, M. Vilette, J.D. Comparot, V. Montouillout, *Appl. Catal. B* 152–153 (2014) 141–149.
- [21] J.D. Song, T.Y. Song, T.T. Zhang, Y. Wang, M.F. Luo, J.Q. Lu, *J. Catal.* 364 (2018) 271–281.
- [22] M. Zieliński, A. Kiderys, M. Pietrowski, I. Tomska-Foralewska, M. Wojciechowska, *Catal. Commun.* 76 (2016) 54–57.
- [23] M. Chen, J.M. Jin, S.D. Lin, Y. Li, W.C. Liu, L. Guo, L. Li, X.N. Li, *J. Fluorine Chem.* 150 (2013) 46–52.
- [24] K. Bourikas, C. Kordulis, A. Lycourghiotis, *Catal. Rev.* 38 (12) (2007) 363–444.
- [25] B.M. Reddy, A. Khan, *Catal. Rev.* 47 (2) (2005) 257–296.
- [26] S. Wuttke, G. Scholz, S. Rüdiger, E. Kemnitz, *J. Mater. Chem.* 17 (2007) 4980–4988.
- [27] E. Kemnitz, S. Wuttke, S.M. Coman, *Eur. J. Inorg. Chem.* (2011) 4773–4794.
- [28] A. Astruc, C. Cochon, S. Dessources, S. Célérier, S. Brunet, *Appl. Catal. A Gen.* 453 (2013) 20–27.
- [29] A. Saberi, Z. Negahdari, S. Bouazza, M. Willert-Porada, *J. Fluorine Chem.* 131 (2010) 1353–1355.
- [30] E. Kemnitz, *Catal. Sci. Technol.* 5 (2015) 786–806.
- [31] W.F. Han, C.P. Zhang, H.L. Wang, S.L. Zhou, H.D. Tang, L.T. Yang, Z.K. Wang, *Catal. Sci. Technol.* 7 (2017) 6000–6012.
- [32] W. Mao, Y.B. Bai, B. Wang, W. Wang, H. Ma, Y. Qin, C. Li, J. Lu, Z.W. Liu, *Appl. Catal. B* 206 (2017) 65–73.
- [33] A.B.D. Nandiyanto, T. Ogi, K. Okuyama, *ACS Appl. Mater. Interfaces* 6 (2014) 4418–4427.
- [34] G. Prieto, H. Tüysüz, N. Duyckaerts, J. Knossalla, G.H. Wang, F. Schüth, *Chem. Rev.* 116 (2016) 14056–14119.
- [35] V.R. Acham, A.V. Biradar, M.K. Dongare, E. Kemnitz, S.B. Umbarkar, *ChemCatChem* 6 (2014) 3182–3191.
- [36] M. Pietrowski, M. Wojciechowska, *J. Fluorine Chem.* 128 (3) (2007) 219–223.
- [37] K. Teinz, S. Wuttke, F. Börno, J. Eicher, *J. Catal.* 282 (2011) 175–182.
- [38] W.Z. Jia, M. Liu, X.W. Lang, C. Hu, J.H. Li, Z.R. Zhu, *Catal. Sci. Technol.* 5 (2015) 3103–3107.
- [39] A. Makarowicz, C.L. Bailey, N. Weiher, E. Kemnitz, S.L.M. Schroeder, S. Mukhopadhyay, A. Wander, B.G. Searle, N.M. Harrison, *Phys. Chem. Chem. Phys.* 11 (2009) 5664–5673.
- [40] C. Stosiek, G. Scholz, S.L.M. Schroeder, E. Kemnitz, *Chem. Mater.* 22 (2010) 2347–2356.
- [41] W.F. Han, S.L. Zhou, M. Xi, H.L. Wang, W.C. Liu, H.D. Tang, Z.K. Wang, C.P. Zhang, *J. Fluorine Chem.* 202 (2017) 65–70.